

# Synthesis of Itaconic Acid Ester Analogues via Self-Aldol Condensation of Ethyl Pyruvate Catalyzed by Hafnium BEA Zeolites

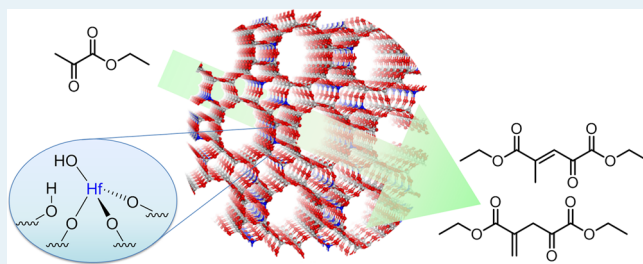
Yuran Wang, Jennifer D. Lewis, and Yuriy Román-Leshkov\*

Department of Chemical Engineering, Massachusetts Institute of Technology, Cambridge, Massachusetts 02139, United States

**S** Supporting Information

**ABSTRACT:** Lewis acidic zeolites are used to synthesize unsaturated dicarboxylic acid esters via aldol condensation of keto esters. Hafnium-containing BEA (Hf-BEA) zeolites catalyze the condensation of ethyl pyruvate into diethyl 2-methyl-4-oxopent-2-enedioate and diethyl 2-methylene-4-oxopentanedioate (an itaconic acid ester analogue) with a selectivity of ca. 80% at ca. 60% conversion in a packed-bed reactor. The catalyst is stable for 132 h on stream, reaching a turnover number of 5110 mol<sub>EP</sub> mol<sub>Hf</sub><sup>-1</sup>. Analysis of the dynamic behavior of Hf-BEA under flow conditions and studies with Na-exchanged zeolites suggest that Hf(IV) open sites possess dual functionality for Lewis and Brønsted acid catalysis.

**KEYWORDS:** itaconic acid ester, aldol condensation, pyruvate, hafnium beta, sodium exchange, open sites, Lewis acidic zeolites



Dicarboxylic acids (diacids) play a central role in the biobased chemicals portfolio, as evidenced by their prevalence in the top 12 chemicals from biomass identified by the U.S. Department of Energy.<sup>1</sup> Diacids are building blocks in condensation polymerization reactions,<sup>2</sup> and their ester forms (diesters) can serve as lubricants, plasticizers, and polymer intermediates.<sup>3</sup> In particular, the unsaturated diacid itaconic acid is a potential biodegradable substitute for high-volume petroleum-derived chemicals such as acrylic acid, maleic anhydride, or acetone cyanohydrin.<sup>4</sup> It can also be used in the production of superabsorbent polymers, synthetic latex, and laminating resins.<sup>4</sup> Although some diacids (e.g., succinic acid) are already produced industrially from biomass, most, including itaconic acid, suffer from prohibitively high production costs.<sup>5–8</sup> Current catalytic routes to synthesize diacids and diesters from biomass-derived molecules, such as Baeyer–Villiger oxidation,<sup>9,10</sup> C–C bond cleavage,<sup>11</sup> and noble-metal-catalyzed aerobic oxidation,<sup>12,13</sup> suffer from poor selectivity,<sup>9,10</sup> inefficient carbon utilization,<sup>11</sup> and/or catalyst deactivation.<sup>12</sup> Flanagan et al. reported a C–C coupling strategy to produce unsaturated dicarboxylic esters through the addition dimerization of crotonates;<sup>14</sup> however, the system depends on homogeneous catalysts.

An alternative route to generate diacids or diesters is via the C–C coupling of keto acids or esters (Scheme 1), which are common intermediates in a myriad of metabolic pathways and can be produced through biocatalysis on a large scale.<sup>7,15–20</sup> Although this coupling strategy is promising, only a few homogeneous catalysts have been shown to activate the carbonyl group adjacent to the ester group.<sup>21–23</sup> However, these catalysts lactonize the aldol adducts instead of generating linear condensation products. Solid base catalysts typically used

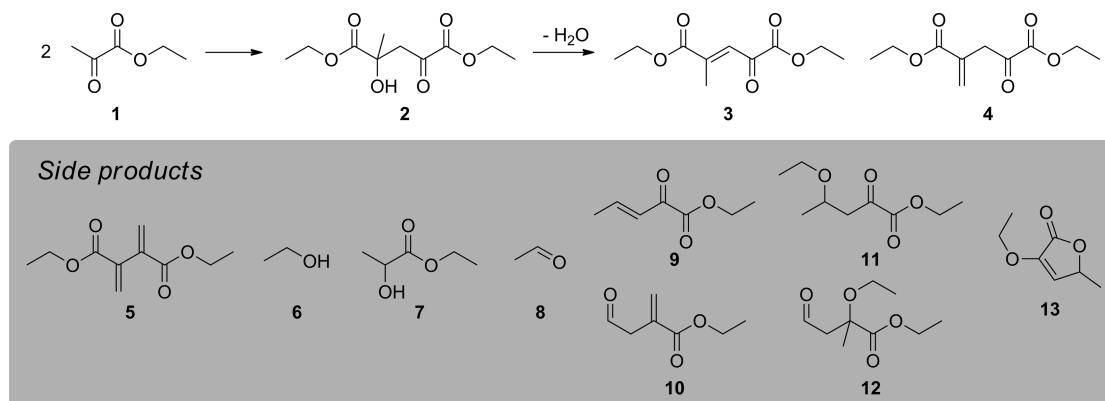
for aldol condensation are not ideal for the proposed system, as they easily deactivate in the presence of organic acids.<sup>24–26</sup>

In this work, we demonstrate a general strategy to synthesize unsaturated dicarboxylic acid esters via the C–C coupling of keto esters with Lewis acidic zeolites. We emphasize the synthesis of itaconic acid ester analogues from the condensation of ethyl pyruvate (EP, 1) (Scheme 1) due to the low thermal stability of pyruvic acid.<sup>27</sup> Zeolites with BEA topology containing Lewis acidic framework heteroatoms, including Sn(IV), Hf(IV) and Zr(IV), can catalyze C–C coupling of biomass-derived oxygenates.<sup>28–31</sup> These materials promote aldol condensation via a soft enolization pathway reminiscent to that observed in class II aldolases.<sup>24</sup> Importantly, these zeolites feature remarkable tolerance to carboxylic acid groups<sup>24</sup> and water,<sup>32,33</sup> making them prime candidates for the biomass-based production of diacids and diesters.

As depicted in Scheme 1, the self-aldol addition of EP 1 followed by dehydration of the aldol addition product, diethyl 2-hydroxy-2-methyl-4-oxopentanedioate 2, results in two diester isomers: diethyl 2-methyl-4-oxopent-2-enedioate 3 and diethyl 2-methylene-4-oxopentanedioate 4. The latter is a functional analogue of itaconic acid ester. In addition to the main coupling reaction, several undesired side reactions are triggered by the presence of acid sites and water generated from the dehydration of aldol adducts. These side reactions (Scheme S1) include hydrolysis of EP to pyruvic acid and ethanol, Meerwein–Ponndorf–Verley (MPV) reduction of EP accompanied by Oppenauer oxidation of ethanol, and aldol reaction

**Received:** February 24, 2016

**Revised:** March 20, 2016

**Scheme 1. Self-Aldol Condensation of Ethyl Pyruvate Catalyzed by Lewis Acidic Zeolites with Products from Side Reactions Listed**

between EP and these side products. Toluene was used as the solvent to suppress side reactions that can occur between EP and alcohols (MPV) or water (hydrolysis).

The catalytic performance of Lewis acidic zeolites for the self-aldol condensation of EP is shown in Table 1. Hf-BEA and

**Table 1. Self-Aldol Condensation of Ethyl Pyruvate Catalyzed by Lewis Acidic Zeolites<sup>a</sup>**

entry	catalyst	EP conversion (%)	selectivity (%) <sup>b</sup>	
			diesters	side products
1	Hf-BEA	80	68	15
2	Zr-BEA	81	64	11
3	Sn-BEA	19	67	6
4	Hf-BEA <sup>c</sup>	78	81	9

<sup>a</sup>Reaction conditions: 3 wt % EP in toluene, EP/metal = 195 (mol/mol), 120 °C, 1 h. <sup>b</sup>selectivity =  $\frac{\sum_i N_{C,i} n_i}{N_{C,EP}(n_{EP,o} - n_{EP})} \times 100\%$ , where  $N_{C,i}$  is the number of carbon atoms in compound  $i$ ,  $n_i$  is the number of moles of compound  $i$  in the reaction mixture, and  $n_{EP,o}$  is the initial moles of EP added. Diesters: 3–5 in Scheme 1. Side products: 6–13 in Scheme 1; distribution for a typical reaction is shown in Figure S7. <sup>c</sup>Calcined in dry air at 550 °C for 5 h after four consecutive runs as shown in Figure S8.

Zr-BEA generate the highest EP conversions (>80%) with comparable selectivities (>64%) to diester products (3–5 in Scheme 1) after 1 h at 120 °C (entries 1 and 2). Sn-BEA shows a lower EP conversion of 19% under identical conditions (entry 3), consistent with previous studies on aldol reactions.<sup>24</sup> Only a ca. 1% conversion is observed from Si-BEA or metal oxides supported on Si-BEA, and a 17% conversion (with 12% selectivity) is obtained for Al-BEA (Table S1, entries 1–7). Collectively, these results indicate that the catalytic activity most likely originates from framework Lewis acidic heteroatoms. In contrast to previously reported homogeneous catalytic systems,<sup>21–23</sup> the lactonization of 2 is not observed with these Lewis acidic zeolites. Nonetheless, compound 13 is likely produced from the lactonization of a C7 molecule (reaction f in Scheme S1), indicating that although lactonization is feasible, the confining effects of the zeolite pores may limit this pathway for larger molecules.<sup>34</sup> Metal oxides with Brønsted basicity typically employed for aldol reactions, including MgO and hydrotalcite,<sup>35</sup> show EP conversions of less than 13% and selectivities of less than 18% (Table S1, entries 8–12). In these systems, pyruvic acid

produced by the hydrolysis of EP is expected to deactivate the basic sites.<sup>24</sup>

Hf-BEA was investigated in further detail due to its superior diester selectivity (68%) at high conversion (80%). The recyclability of Hf-BEA was probed by washing with toluene and reusing the material for five consecutive batch reactions at 120 °C. After a gradual conversion decrease from 80% (run 1) to 60% (run 4), the catalyst shows no further conversion drop in run 5 (Figure S8). Remarkably, calcination of the catalyst under dry air after run 4 improves the diester selectivity from 68% to 81% in addition to recovering the initial activity (Table 1, entry 4). This unique behavior prompted us to further investigate the stability and regeneration of Hf-BEA for EP coupling under flow conditions.

Figure 1 shows EP conversion and selectivities to diesters and side products catalyzed by Hf-BEA as a function of time on stream (TOS) in a packed bed reactor (see Figure S10 for yields). Hf-BEA was calcined in situ under dry air at 550 °C for 5 h prior to feeding the reactants. The catalyst bed was

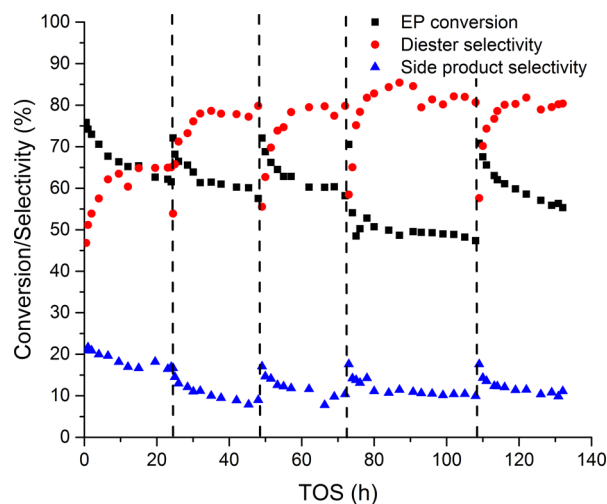


**Figure 1.** EP conversion and selectivity to diesters and side products as a function of time on stream (TOS) for the flow reaction with Hf-BEA. Reaction conditions: 120 °C, 12 bar, 320 mg of Hf-BEA, 3 wt % EP in toluene, flow rate 0.20 mL min<sup>-1</sup>, WHSV 32.2 h<sup>-1</sup>. Dashed lines represent regeneration of Hf-BEA: flush with toluene at 120 °C, dry under N<sub>2</sub> at 150 °C, and calcine with dry air at 550 °C for 5 h. Diesters: 3–5 in Scheme 1. Side products: 6–13 in Scheme 1; distributions are shown in Figure S9.

Table 2. Self-Aldol Condensation of Ethyl Pyruvate Catalyzed by Na-Exchanged and Acid-Washed Hf-BEA<sup>a</sup>

entry	catalyst	treatment	Si/Hf ratio <sup>c</sup>	Na/Hf molar ratio <sup>d</sup>	micropore volume (cm <sup>3</sup> g <sup>-1</sup> )	EP conv. (%)	selectivity (%) <sup>b</sup>	
							diesters	side products
1	Hf-BEA	None	115	n/a	0.20	77	69	7
2	Hf-BEA-Na-1 <sup>e</sup>	NaNO <sub>3</sub> (1 M)	116	0.69	0.17	15	34	10
3	Hf-BEA-Na-2 <sup>f</sup>	NaOH (pH = 10)	113	0.02	0.20	59	70	7
4	Hf-BEA-AW-1 <sup>g</sup>	H <sub>2</sub> SO <sub>4</sub> (1 M)	115	n.d.	0.20	74	69	12
5	Hf-BEA-AW-2 <sup>g</sup>	H <sub>2</sub> SO <sub>4</sub> (1 M)	119	n.d.	0.19	77	79	7

<sup>a</sup>Reaction conditions same as in Table 1, but with a different batch of Hf-BEA zeolite. <sup>b</sup>Selectivity same as defined in Table 1. <sup>c</sup>No significant changes in Si/Hf ratios after different treatments, indicating the treatments do not cause Hf leaching. <sup>d</sup>n/a, not applicable. n.d., not detected. <sup>e</sup>Hf-BEA after Na exchange treatment 1 with NaNO<sub>3</sub> (1 M). <sup>f</sup>Hf-BEA after Na exchange treatment 2 with NaOH (pH = 10). <sup>g</sup>Hf-BEA-Na-1 or Hf-BEA-Na-2 washed with H<sub>2</sub>SO<sub>4</sub> (1 M) at room temperature for 1 h, recovered, and then calcined at 550 °C. Full details on material synthesis available in Section S1.

regenerated by calcination under identical conditions over the course of the experiment; each cycle is indicated by the dashed lines in Figure 1. The reactor was operated at 120 °C with a weight hourly space velocity (WHSV) of 32.2 h<sup>-1</sup>. Steady-state conversions of ca. 60%, selectivities toward diesters of ca. 80%, and a total turnover number of 5110 mol<sub>EP</sub> mol<sub>Hf</sub><sup>-1</sup> over 132 h on stream were observed. Elemental analysis of the spent catalyst showed no detectable change in Hf content (Table S3), and powder X-ray diffraction confirmed that the long-range crystallinity was preserved (Figure S13). N<sub>2</sub> adsorption data of the spent catalyst showed a slightly smaller micropore volume (0.17 cm<sup>3</sup> g<sup>-1</sup>) than that of the pristine catalyst (0.19 cm<sup>3</sup> g<sup>-1</sup>) (Table S3, Figure S16).

After each calcination, transient and steady-state regimes are clearly observed in the reactivity data (Figure 1 and Figure S10). During the transient periods, the EP conversion decreases by ca. 10% over 10 h TOS, while the diester selectivity increases by ca. 20% and the selectivity to side products decreases by ca. 5%. The decrease in EP conversion and the increase in diester selectivity appear to be correlated with a decrease in the rates of side reactions that are initiated by hydrolysis (Scheme S1), indicating the deactivation of active sites responsible for hydrolysis reactions. The steady-state period, which accounts for the remaining 14–26 h on stream, is characterized by less than 5% decrease in EP conversion and stable selectivity to diesters (Figure 1). Calcination of the catalyst bed results in a partial recovery of hydrolysis activity, demonstrating that deactivation of hydrolysis active sites is partially reversible. The regeneration by calcination coupled with the 5 wt % loss observed by thermogravimetric analysis of the catalyst recovered after 132 h TOS suggests that interaction of organic molecules with the sites contributes to the apparent decrease in hydrolysis rates.

The increased diester yield coupled with the concurrent decrease of hydrolysis activity in the transient regimes suggests that different moieties in the active site ensemble catalyze the aldol condensation and hydrolysis reactions. Control batch reactions with Si-BEA (Table S1, entries 4–5) showed no activity, thus pointing to the involvement of Hf in generating these sites. In addition to Lewis acidity, spectroscopic evidence<sup>36</sup> and computational studies<sup>37–39</sup> suggest the presence of weak Brønsted acidity associated with the silanol moiety of monohydrolyzed framework heteroatom sites (i.e., open sites) in Lewis acidic zeolites. Thus, these weak Brønsted acid sites are likely responsible for hydrolysis, and selective deactivation of the acidic proton due to alkoxide formation could explain the transient deactivation of hydrolysis. Indeed, similar deactivation behavior has been observed in previous flow studies of Lewis

acidic zeolites.<sup>40,41</sup> Lewis et al. showed through Sn- or Hf-BEA catalyzed tandem reactions between 5-(hydroxymethyl)furfural and alcohols that Lewis acid-catalyzed transfer hydrogenation activity remained unchanged, whereas Brønsted acid-catalyzed etherification activity decreased over time and could be partially recovered by calcination.<sup>40</sup> Importantly, <sup>13</sup>C{<sup>1</sup>H} cross-polarization magic-angle-spinning nuclear magnetic resonance (CP MAS NMR) of the spent catalyst showed alkoxide species formation on silanol groups in the zeolite.<sup>40</sup>

An important feature demonstrated in the flow data is the increase in selectivity toward diesters after the first regeneration by calcination (Figure 1, after 24 h TOS) that is consistent with the increase in selectivity observed after calcination in the batch studies. Specifically, the steady-state diester selectivity increases from 65% to 79% (yield: 42% to 48%), and the steady-state selectivity to side products decreases from 17% to 10% (yield: 11% to 5%). However, no further improvement in diester selectivity is observed after successive calcinations. This irreversible shift in selectivity after the first regeneration is indicative of permanent changes to the catalyst active sites that contribute to the decrease in hydrolysis activity, the increase in aldol condensation activity, or a combination of both.

The dynamic behavior exhibited by Hf-BEA in flow is consistent with prior studies of Lewis acidic zeolites that suggest amorphization and site restructuring are responsible for changes in activity and selectivity after extended TOS.<sup>30,40,41</sup> Specifically, for aqueous dihydroxyacetone isomerization, Lari et al. observed an 18% loss in crystallinity for Sn-BEA and a 16% decrease in tetrahedral coordination for Sn-MFI after 24 h TOS.<sup>41</sup> Lewis et al. demonstrated with <sup>119</sup>Sn MAS and <sup>119</sup>Sn{<sup>1</sup>H} CP MAS NMR that open and distorted framework Sn sites were generated in <sup>119</sup>Sn-BEA during the transfer hydrogenation and etherification of 5-(hydroxymethyl)furfural with ethanol, while only closed sites were observed in the pristine catalyst.<sup>40</sup> Studies by Boronat et al. and Bermejo-Deval et al. also suggest that the distribution of open and closed sites in Sn-BEA changes with postsynthesis treatment (e.g., calcination or exposure to reaction conditions).<sup>42,43</sup>

The molecular connectivity of active sites (i.e., open versus closed) has been suggested to affect catalytic activity and selectivity due to differences in Lewis acidity, flexibility, and functionality of the neighboring silanol group.<sup>42–46</sup> Bermejo-Deval et al. demonstrated with Na-treated Sn-BEA that the cations likely exchange onto silanol groups proximal to Sn(IV) open sites.<sup>45</sup> The presence of Na<sup>+</sup> alters the glucose isomerization reaction pathway from a fructose-producing 1,2-hydrate shift to a mannose-producing 1,2-carbon shift, and the effect can be reversed by washing with a H<sub>2</sub>SO<sub>4</sub> solution to



remove the Na<sup>+</sup> cations.<sup>45</sup> Computational studies indicate that the change in product distribution is a consequence of the electrostatic stabilization of the carbon shift relative to hydride shift caused by the presence of Na<sup>+</sup> ions at the open Sn center.<sup>47</sup> To probe the nature of the active sites in Hf-BEA, we conducted a preliminary study with Na-exchanged Hf-BEA. Specifically, two Na-exchanged Hf-BEA catalysts were prepared using methods adapted from the work of Bermejo-Deval et al. (see Section S1).<sup>45</sup> These samples were denominated as Hf-BEA-Na-1 and Hf-BEA-Na-2, with Na/Hf molar ratios of 0.69 and 0.02, respectively (Table 2). Batch reactions catalyzed by Hf-BEA-Na-1 resulted in 15% EP conversion and ca. 34% selectivity to diesters (Table 2 and S2, entry 2). This significant reduction in activity and selectivity is unlikely a result of pore blockage (Section S2). Despite its low Na content, Hf-BEA-Na-2 resulted in a diminished EP conversion of 59% when compared to the 77% conversion generated by pristine Hf-BEA (Tables 2 and S2, entry 3). The catalyst performance and pore volume of both Na-exchanged zeolites were recovered by washing with H<sub>2</sub>SO<sub>4</sub> (Tables 2 and S2, entries 4–5). This reversible activity drop is likely caused by a strong interaction between Na<sup>+</sup> and the active sites, which we investigate further using Fourier transform infrared (FTIR) spectroscopy with deuterated acetonitrile (CD<sub>3</sub>CN) adsorption.

FTIR spectra of CD<sub>3</sub>CN adsorbed on pristine Hf-BEA show the characteristic bands seen with M-BEA zeolites (Figure 2a).<sup>42,45,48</sup> The C≡N stretching vibrations of CD<sub>3</sub>CN at 2310, 2275, and 2268 cm<sup>-1</sup> are representative of CD<sub>3</sub>CN that is strongly bound to Lewis acid sites (i.e., tetrahedral Hf(IV) centers), coordinated to silanol groups, and physisorbed, respectively.<sup>42,45</sup> The band at 2310 cm<sup>-1</sup> appears to be a single peak, which differs from previous reports of two bands corresponding to open and closed sites for Sn-BEA.<sup>42,45</sup> However, these data are consistent with studies of Zr-BEA that show only one band in this region.<sup>36</sup> Na exchange results in a decrease in the band at 2310 cm<sup>-1</sup> and the appearance of a new band at 2284 cm<sup>-1</sup>, which has previously been assigned as CD<sub>3</sub>CN adsorbed on Na-exchanged open sites for Sn-BEA.<sup>45</sup> This change is more prominent for the material with a higher degree of Na exchange (Hf-BEA-Na-1, Figure 2b) than for the material with low Na loading (Hf-BEA-Na-2, Figure S18a). Controls with Na-exchanged Si-BEA (Si-BEA-Na) confirm that framework Hf(IV) is required to observe this feature (Figure S18b).<sup>49</sup> After acid wash, the FTIR spectra resemble again those of the pristine material, demonstrating the reversibility of the Na exchange (Figure 2c).

Assuming that Na<sup>+</sup> interacts with the open framework Hf(IV) site in a similar manner to that proposed by Bermejo-Deval et al. for Sn-BEA,<sup>45</sup> we hypothesize that the open sites are the main active sites for aldol condensation. Thus, open site ensembles likely have 2-fold functionality: the Lewis acidic character of the heteroatom catalyzes the aldol reaction, whereas the Brønsted acidic silanol group catalyzes hydrolysis. The change in the chemical environment of the open site upon Na exchange—evidenced by the change in the FTIR band corresponding to CD<sub>3</sub>CN adsorbed on Hf(IV) sites from 2310 to 2284 cm<sup>-1</sup>—may explain the lower reactivity of Na-exchanged Hf-BEA for aldol condensation. However, the presence and catalytic contribution of Hf(IV) closed sites cannot be excluded. Detailed characterization and kinetics studies are currently underway to confirm these hypotheses.

In summary, we have developed a new approach to synthesize unsaturated dicarboxylic acid esters from keto esters

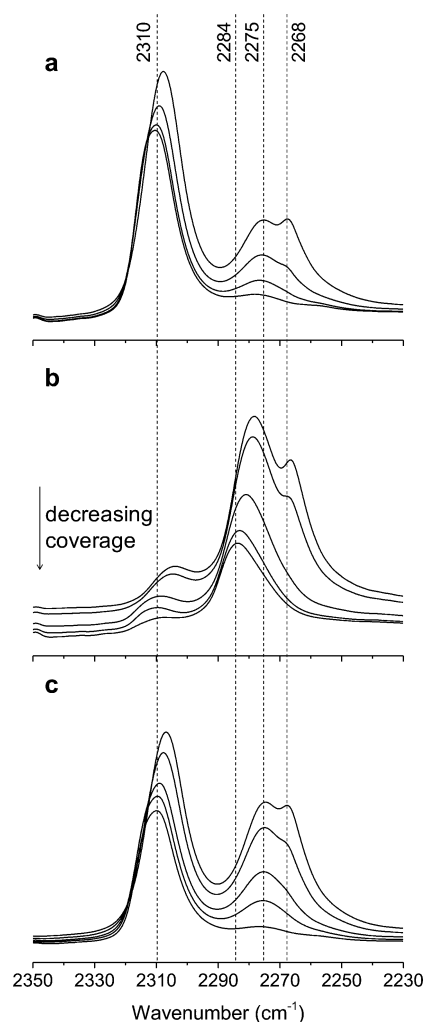


**Figure 2.** FTIR spectra with decreasing CD<sub>3</sub>CN coverage on (a) Hf-BEA, (b) Hf-BEA-Na-1, and (c) Hf-BEA-AW-1. Signals are referenced to the bare material and normalized by the combination and overtone modes of zeolite Si–O–Si stretches (1750–2100 cm<sup>-1</sup>). Reference lines are for physisorbed CD<sub>3</sub>CN (2268 cm<sup>-1</sup>) and CD<sub>3</sub>CN adsorbed on silanols (2275 cm<sup>-1</sup>), Na-exchanged open Hf(IV) sites (tentative, 2284 cm<sup>-1</sup>), and Lewis acidic Hf sites (2310 cm<sup>-1</sup>).

via aldol condensation catalyzed by Lewis acidic zeolites. In particular, we demonstrate that Hf-BEA can catalyze the self-aldol condensation of EP in toluene to produce itaconic acid ester analogues. The catalyst is stable for 132 h TOS in a packed-bed reactor with a diester selectivity of ca. 80% at 120 °C. Na exchange substantially decreases Hf-BEA activity and significantly alters the FTIR band for CD<sub>3</sub>CN adsorbed on the framework Hf(IV) sites, indicating a strong interaction between Na<sup>+</sup> and the active sites. The open framework Hf(IV) site is hypothesized to possess strong Lewis acidity and weak Brønsted acidity that are responsible for the dual functionality of the catalyst. However, further investigation is needed to fully elucidate the nature of the active site and guide catalyst and reaction optimization.

## ■ ASSOCIATED CONTENT

### Supporting Information

The Supporting Information is available free of charge on the ACS Publications website at DOI: 10.1021/acscatal.6b00561.

Experimental procedures for catalyst synthesis, characterization, and test reactions; side reaction scheme; a typical GC chromatogram for reaction mixtures; MS data for reaction products; additional reaction data for batch studies, flow studies, and Na exchange studies; and catalyst characterization data (ICP-MS, PXRD, N<sub>2</sub> adsorption–desorption and FTIR) (PDF)

## AUTHOR INFORMATION

### Corresponding Author

\*E-mail: yroman@mit.edu.

### Notes

The authors declare no competing financial interest.

## ACKNOWLEDGMENTS

This work was sponsored by the Chemical Sciences, Geosciences and Biosciences Division, Office of Basic Energy Sciences, Office of Science, U.S. Department of Energy, under Award No. DE-FG0212ER16352. J.D.L. was partially supported by the National Science Foundation Graduate Research Fellowship under Grant No. 122374. Any opinion, findings, and conclusions or recommendations expressed in this material are those of the authors and do not necessarily reflect the views of the National Science Foundation.

## REFERENCES

- (1) Werpy, T.; Petersen, G.; Aden, A.; Bozell, J.; Holladay, J.; White, J.; Manheim, A.; Eliot, D.; Lasure, L.; Jones, S. *Top value added chemicals from biomass. Vol. 1-Results of screening for potential candidates from sugars and synthesis gas*; Department of Energy: Washington, DC, 2004.
- (2) Dicarboxylic Acids, Aliphatic. Ullmann's Encyclopedia of Industrial Chemistry [Online]; Wiley-VCH Verlag GmbH & Co. KGaA, Posted November 19, 2014. [http://onlinelibrary.wiley.com/doi/10.1002/14356007.a08\\_523.pub3/pdf](http://onlinelibrary.wiley.com/doi/10.1002/14356007.a08_523.pub3/pdf).
- (3) Dicarboxylic Acids. Kirk-Othmer Encyclopedia of Chemical Technology [Online]; John Wiley & Sons, Inc., Posted September 17, 2010. <http://onlinelibrary.wiley.com/doi/10.1002/0471238961.0409030110150814.a01.pub2/pdf>.
- (4) WEASTRA s.r.o, Management Consultancy. WP 8.1. Determination of market potential for selected platform chemicals. Itaconic acid, succinic acid, 2,5-furandicarboxylic acid; WEASTRA s.r.o., 2012. <http://www.bioconcept.eu/deliverables/>.
- (5) Okabe, M.; Lies, D.; Kanamasa, S.; Park, E. Y. *Appl. Microbiol. Biotechnol.* **2009**, *84*, 597–606.
- (6) Steiger, M. G.; Blumhoff, M. L.; Mattanovich, D.; Sauer, M. *Front. Microbiol.* **2013**, *4*, 23.
- (7) Straathof, A. J. *Chem. Rev.* **2014**, *114*, 1871–1908.
- (8) Mondala, A. H. *J. Ind. Microbiol. Biotechnol.* **2015**, *42*, 487–506.
- (9) Wang, Y. R.; Vogelgsang, F.; Roman-Leshkov, Y. *ChemCatChem* **2015**, *7*, 916–920.
- (10) Dutta, S.; Wu, L. L.; Mascall, M. *Green Chem.* **2015**, *17*, 2335–2338.
- (11) Liu, J.; Du, Z.; Lu, T.; Xu, J. *ChemSusChem* **2013**, *6*, 2255–2258.
- (12) Wang, Y. R.; Van de Vyver, S.; Sharma, K. K.; Roman-Leshkov, Y. *Green Chem.* **2014**, *16*, 719–726.
- (13) Casanova, O.; Iborra, S.; Corma, A. *ChemSusChem* **2009**, *2*, 1138–1144.
- (14) Flanagan, J. C. A.; Kang, E. J.; Strong, N. I.; Waymouth, R. M. *ACS Catal.* **2015**, *5*, 5328–5332.
- (15) Wieschalka, S.; Blombach, B.; Bott, M.; Eikmanns, B. *J. Microbiol. Biotechnol.* **2013**, *6*, 87–102.
- (16) Li, Y.; Chen, J.; Lun, S. Y. *Appl. Microbiol. Biotechnol.* **2001**, *57*, 451–459.
- (17) Schwartz, T. J.; Shanks, B. H.; Dumesic, J. A. *Curr. Opin. Biotechnol.* **2016**, *38*, 54–62.
- (18) Dusselier, M.; Van Wouwe, P.; Dewaele, A.; Makshina, E.; Sels, B. F. *Energy Environ. Sci.* **2013**, *6*, 1415–1442.
- (19) Il'Chenko, A.; Shcherbakova, V. *Microbiology* **2008**, *77*, 430–435.
- (20) Johnson, C. W.; Beckham, G. T. *Metab. Eng.* **2015**, *28*, 240–247.
- (21) Gathergood, N.; Juhl, K.; Poulsen, T. B.; Thordrup, K.; Jorgensen, K. A. *Org. Biomol. Chem.* **2004**, *2*, 1077–1085.
- (22) Dambrouso, P.; Massi, A.; Dondoni, A. *Org. Lett.* **2005**, *7*, 4657–4660.
- (23) Sun, Y.; Chen, H.; Li, Z.; Wang, Q.; Tao, F. *Synthesis* **2008**, *2008*, 589–593.
- (24) Lewis, J. D.; Van de Vyver, S.; Roman-Leshkov, Y. *Angew. Chem., Int. Ed.* **2015**, *54*, 9835–9838.
- (25) Podrebarac, G. G.; Ng, F. T. T.; Rempel, G. L. *Chem. Eng. Sci.* **1997**, *52*, 2991–3002.
- (26) *New Solid Acids and Bases: Their Catalytic Properties*; Tanabe, K.; Misono, M.; Ono, Y.; Hattori, H., Eds.; Elsevier Science Publishing Company, Inc.: New York, NY, 1989; p 339.
- (27) Frey, H. *Thermal decomposition of pyruvic acid and its esters leading to CO<sub>2</sub>*; University of California, Berkeley, Radiation Lab: Berkeley, California, 1956.
- (28) Mahmoud, E.; Yu, J. Y.; Gorte, R. J.; Lobo, R. F. *ACS Catal.* **2015**, *5*, 6946–6955.
- (29) Van de Vyver, S.; Román-Leshkov, Y. *Angew. Chem., Int. Ed.* **2015**, *54*, 12554–12561.
- (30) Van de Vyver, S.; Odermatt, C.; Romero, K.; Prasomsri, T.; Román-Leshkov, Y. *ACS Catal.* **2015**, *5*, 972–977.
- (31) Holm, M. S.; Pagan-Torres, Y. J.; Saravanamurugan, S.; Riisager, A.; Dumesic, J. A.; Taarning, E. *Green Chem.* **2012**, *14*, 702–706.
- (32) Moliner, M.; Roman-Leshkov, Y.; Davis, M. E. *Proc. Natl. Acad. Sci. U. S. A.* **2010**, *107*, 6164–6168.
- (33) Roman-Leshkov, Y.; Moliner, M.; Labinger, J. A.; Davis, M. E. *Angew. Chem., Int. Ed.* **2010**, *49*, 8954–8957.
- (34) De Clercq, R.; Dusselier, M.; Christiaens, C.; Dijkmans, J.; Iacobescu, R. I.; Pontikes, Y.; Sels, B. F. *ACS Catal.* **2015**, *5*, 5803–5811.
- (35) Sacia, E. R.; Balakrishnan, M.; Deaner, M. H.; Goulas, K. A.; Toste, F. D.; Bell, A. T. *ChemSusChem* **2015**, *8*, 1726–1736.
- (36) Sushkevich, V. L.; Vimont, A.; Travert, A.; Ivanova, I. I. *J. Phys. Chem. C* **2015**, *119*, 17633–17639.
- (37) Montejo-Valencia, B. D.; Salcedo-Pérez, J.; Curet-Arana, M. C. *J. Phys. Chem. C* **2016**, *120*, 2176–2186.
- (38) Yang, G.; Zhou, L.; Han, X. *J. Mol. Catal. A: Chem.* **2012**, *363*, 371–379.
- (39) Yang, G.; Lan, X. J.; Zhuang, J. Q.; Ma, D.; Zhou, L. J.; Liu, X. C.; Han, X. W.; Bao, X. H. *Appl. Catal., A* **2008**, *337*, 58–65.
- (40) Lewis, J. D.; Van de Vyver, S.; Crisci, A. J.; Gunther, W. R.; Michaelis, V. K.; Griffin, R. G.; Roman-Leshkov, Y. *ChemSusChem* **2014**, *7*, 2255–2265.
- (41) Lari, G.; Dapsens, P.; Scholz, D.; Mitchell, S.; Mondelli, C.; Pérez-Ramírez, J. *Green Chem.* **2016**, *18*, 1249–1260.
- (42) Boronat, M.; Concepcion, P.; Corma, A.; Renz, M.; Valencia, S. *J. Catal.* **2005**, *234*, 111–118.
- (43) Bermejo-Deval, R.; Assary, R. S.; Nikolla, E.; Moliner, M.; Roman-Leshkov, Y.; Hwang, S. J.; Palsdottir, A.; Silverman, D.; Lobo, R. F.; Curtiss, L. A.; Davis, M. E. *Proc. Natl. Acad. Sci. U. S. A.* **2012**, *109*, 9727–9732.
- (44) Sushkevich, V. L.; Palagin, D.; Ivanova, I. I. *ACS Catal.* **2015**, *5*, 4833–4836.
- (45) Bermejo-Deval, R.; Orazov, M.; Gounder, R.; Hwang, S. J.; Davis, M. E. *ACS Catal.* **2014**, *4*, 2288–2297.
- (46) Harris, J. W.; Cordon, M. J.; Di Iorio, J. R.; Vega-Vila, J. C.; Ribeiro, F. H.; Gounder, R. *J. Catal.* **2016**, *335*, 141–154.
- (47) Christianson, J. R.; Caratzoulas, S.; Vlachos, D. G. *ACS Catal.* **2015**, *5*, 5256–5263.
- (48) Roy, S.; Bakhmutsky, K.; Mahmoud, E.; Lobo, R. F.; Gorte, R. J. *ACS Catal.* **2013**, *3*, 573–580.

(49) Yu, J.; Luo, J.; Zhang, Y.; Cao, J.; Chang, C.-C.; Gorte, R.; Fan, W. *Microporous Mesoporous Mater.* **2016**, *225*, 472–481.